NON-GAUSSIAN CLUSTERING OF SAR IMAGES FOR GLACIER CHANGE DETECTION

Vahid Akbari, Anthony Doulgeris, and Torbjørn Eltoft

Department of Physics and Technology, University of Tromsø, 9037,Tromsø, Norway
Email: vahid.akbari@uit.no, anthony.p.doulgeris@uit.no, torbjorn.eltoft@uit.no

ABSTRACT

Our aim is to use unsupervised, non-Gaussian clustering of Arctic glaciers for post-classification change detection. Firstly, we demonstrate the consistency of non-Gaussian clustering algorithms for Envisat ASAR images by characterizing the expected random error level for different SAR acquisition conditions (such as incidence angle).This allows us to determine whether an observed variation is statistically significant and therefore can be used for post-classification change detection of Arctic glaciers. Real significant change was not detected with mixed configurations during the time period of this study.

Key words: SAR; Clustering; Glacier; Change Detection; Non-Gaussian; Statistical modeling.

1. INTRODUCTION

Changes in the Arctic glaciers and ice caps provide a visible manifestation of climate change. Being recognized as potentially the largest short term contributors to sea level rise and having been observed to be one of the fastest warming areas on the planet [1], the present state of the Arctic ice masses, and changes over time, are of scientific and social importance.

As climate changes, so too do the variables affecting glaciers. Identifying and monitoring fluctuations in glacier facies provides a means to track climate change. The only feasible method to obtain good spatial and temporal coverage of the Arctic glaciers is through the use of satellites. Space-borne SAR instruments, operating independently of weather and daylight, are a particularly valuable tool in Arctic areas. SAR has an added advantage over higher frequency instruments (visible and laser) because the signal penetrates some distance into the glacier such that the return signal is influenced not only by the surface, but also by the shallow subsurface.

Pixel-wise analysis of SAR imagery is generally complicated due to the presence of speckle and requires that statistical modeling methods are employed. It is well known that radar speckle is often non-Gaussian in distribution. For this reason, various non-Gaussian models have been proposed to represent SAR data [2]. These have later been extended into the polarimetric realm, where the multivariate K-distributions [3, 4] and G-distributions [5] are successful examples. Both these distributions are members of the so-called product model, which states that, under certain conditions, the backscattered signal results from the product between a Gaussian speckle noise component and the terrain backscatter. Associated with these models is a so-called non-Gaussianity parameter, which accounts for deviation from Gaussian statistics.

The analysis utilizes several Envisat ASAR, dual-pol scenes over Kongsvegen glacier, Svalbard (See Fig. 1) [6], from winter 2004, 2005 and 2006, together with some ground based field observations. In this study, we use the non-Gaussian based K-Wishart clustering algorithm to segment each SAR scene into several glacier classes. Ground truth data are used to reduce the number of classes of segmented images into four major ground truth classes and to investigate the accuracy of classification.

We demonstrate consistency by comparing scenes close together in time and from different acquisition parameters (e.g. incidence angle). Subsequent yearly classifications are discussed in terms of post-classification change detection, by directly observing differences in the classified images. These procedures may form the basis for more operational monitoring of Arctic areas.

This paper is organized as follows: In section 2 and section 3 we introduce GPR data profiles as a set of ground truth data and SAR images in different acquisitions as a satellite data set, respectively. Section 4 demonstrates the product model used in this study. Section 5 identifies the KW-distribution for statistical modeling and the use of this distribution in a Baysian classifier is introduced in section 6. Then in sections 7 and 8, we look at the results of unsupervised classification, classification accuracy and change detection. Finally, conclusions on the presented research are given in the last section.

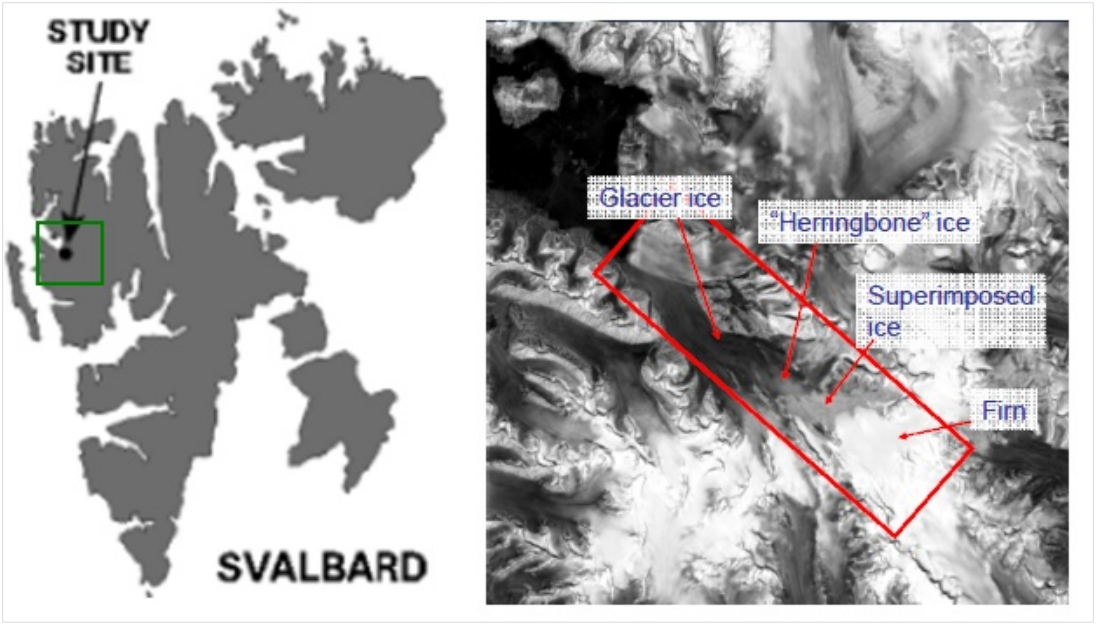

Figure 1. The left image shows the location of our case study in Svalbard and the right image is a combined SAR intensity image showing the four zone of interest .

2. GROUND TRUTH DATA

Ground truth data are derived from a network of ground penetrating radar (GPR) profiles collected in 2005. The along glacier profiles have been manually classified into 4 zones of interest [6] in Fig. 2. These zones include glacier ice, herringbone ice, superimposed ice and firn. These GPR data profiles have been overlaid onto one of the classified image as can be seen in Fig. 4. We use GPR profiles to reduce the classified images different number of classes into these four major ground truth classes and obtain an overall classification accuracy. Since these class labels now match on all images, we subsequently investigate changes in the firn class alone for consistency and time series analysis.

3. SATELLITE DATA SET

Our data consist of a time series of yearly winter SAR images for the period 2004-2006 with different acquisition configurations over Kongsvegen glacier, Svalbard. We have available 118 dual polarization C-band Envisat ASAR images in AP mode from both ascending and descending orbits and in both HH/HV and VV/VH polarizations, over a large range of incidence angles from 14 to 43 degrees (swath angles IS1 to IS7). The SAR acquisition conditions affect backscatter from different objects and glacier facies and we can have variation from differing:

- Polarisation (Dual polarised: VV/VH or HH/HV)
- Incidence angles (IS1 to IS7)
- Orbit (ascending or descending passes)

The raw single-look complex (SLC) data is geo-coded and multi-looked simultaneously to produce 30m resolution, 96-look covariance matrix data (MLC) images. A mask is applied to isolate the glacier pixels for classification.

4. PRODUCT MODEL

After multi-looking, our image data consist of multi-look complex (MLC) matrix data, $\mathbf{C}$, which are the covariance matrices of the raw scattering coefficients, $\mathbf{S}$.

$$\mathbf{C} = \frac{1}{L}\sum_{l=1}^{L}\mathbf{S}_l\mathbf{S}_l^H = \begin{bmatrix} \mathbf{C}_{XXXX} & \mathbf{C}_{XXXY} \\ \mathbf{C}^*_{XXXY} & \mathbf{C}_{XYXY} \end{bmatrix}, \quad (1)$$

where L is the number of looks. The non-Gaussian product model describes the covariance matrix data as the product of a non-Gaussian *texture* term and a Wishart distributed *speckle* term [7]. Assuming that the texture has higher spatial correlation than the speckle over small local neighborhoods, our MLC product model can be written:

$$\mathbf{C} = Z\mathbf{W}_{L,\Gamma}; \qquad \mathbf{W}_{L,\Gamma} \sim Wishart(L, \mathbf{\Gamma}). \quad (2)$$

The non-Gaussian nature of the product model depends on the specific model for the scalar texture variable Z [8, 7].

5. K-WISHART DISTRIBUTION

If the texture term of the product model is given by the gamma distribution with probability density function

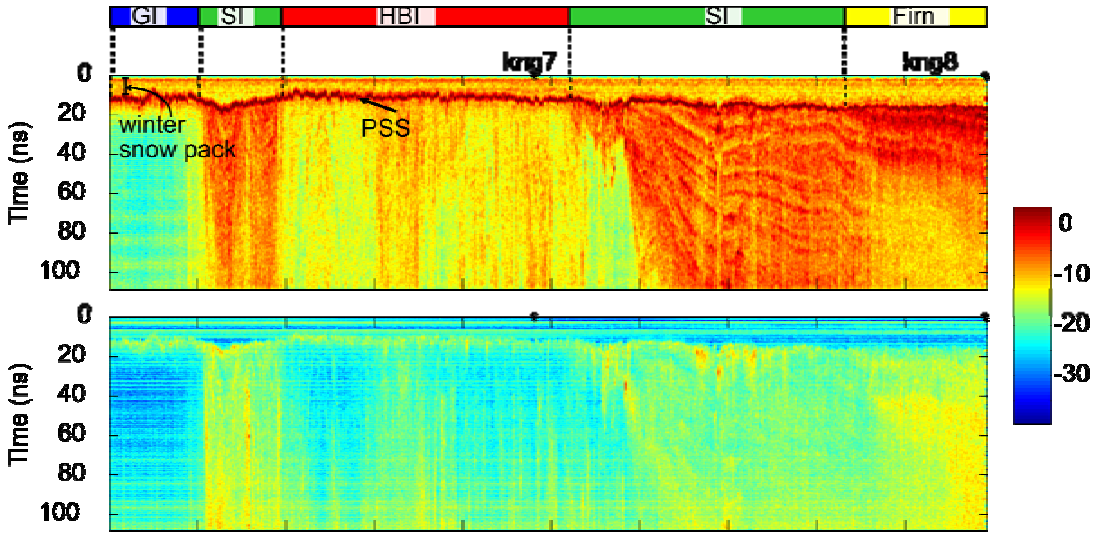

Figure 2. (a) GPR copolarized radar cross section. (b) GPR cross-polarized radar cross section. The different glacier zones are labeled in the color bar at the top. Blue = glacier ice (GI), red = herringbone ice (HBI), green = superimposed ice (SI), and yellow = firn [6].

(pdf) given by

$$p(Z;\mu,\alpha) = \left(\frac{\alpha}{\mu}\right)^{\alpha} \frac{Z^{\alpha-1}}{\Gamma(\alpha)} \exp(-\frac{\alpha}{\mu}Z), \qquad (3)$$

then the marginal distribution for C may be obtained by integrating the conditional pdf over the prior distribution of Z, that is

$$p(\mathbf{C}) = \int p(\mathbf{C}|Z)p(Z)dZ; \qquad \mathbf{C}|Z \sim W_C(L,\mathbf{\Gamma}). \qquad (4)$$

The resulting distribution is known as the K-Wishart distribution [8] and in closed form is:

$$\begin{aligned} &\mathrm{KW}(\mathbf{C};L,\mu,\alpha,\mathbf{\Gamma}) \\ &= \frac{2|\mathbf{C}|^{L-d}}{\mathrm{I}(L,d)\Gamma(\alpha)} \left(\frac{L\alpha}{\mu}\right)^{\frac{\alpha+Ld}{2}} \left(tr(\mathbf{\Gamma}^{-1}\mathbf{C})\right)^{\frac{\alpha-Ld}{2}} \\ &\times \mathrm{K}_{\alpha-Ld}\left(2\sqrt{\frac{L\alpha}{\mu}tr(\mathbf{\Gamma}^{-1}\mathbf{C})}\right), \end{aligned} \qquad (5)$$

where $tr(\cdot)$ and $|\cdot|$ denote the trace operation and determinant, respectively, and $I(L,d)$ is a normalization constant

$$I(L,d) = \pi^{\frac{d(d-1)}{2}} \prod_{i=1}^{d} \Gamma(L-i+1). \qquad (6)$$

Note that the probability expression is influenced by the shape α , the width μ, the number of looks L and polarimetric covariance structure matrix $\mathbf{\Gamma}$ [9]

6. BAYSIAN CLASSIFIER

In the previous section, we introduced the K-Wishart distribution along with its defining parameters. Here we apply this distribution in a Bayesian classifier [8]. We want to assign each pixel to a specific class based upon the posterior probability for the class ω_j among the set of possible outcomes $\omega_1, \omega_2, ..., \omega_k$. Using Bayes's rule:

$$P(\omega_j|\mathbf{C};\alpha_j,\mu_j,\mathbf{\Gamma}_j) \propto \mathrm{KW}(\mathbf{C}|\omega_j;\alpha_j,\mu_j,\mathbf{\Gamma}_j)P(\omega_j), \qquad (7)$$

where $P(\omega_j|\mathbf{C};\alpha_j,\mu_j,\mathbf{\Gamma}_j)$ is the posterior probability of class membership, i.e., the probability that $\mathbf{C}$ belongs to ω_j given the observation $\mathbf{C}$. Using Bayes' rule above, we label a new case $\mathbf{C}$ with a class ω_j that achieves the highest posterior probability.

Unsupervised segmentation of C matrices is achieved using a modified expectation-maximization (EM) approach, which includes an additional goodness-of-fit test stage. The standard EM-algorithm consists of an E-step that estimates class likelihoods using K-Wishart distribution and an M-step that updates all class parameters [10]. Our modification is to include a regular goodness-of-fit test stage to split 'bad' classes and merge 'virtually identical' competing classes [11]. This ensures that the final clusters are all good model fits, and also dynamically determines the appropriate number of significant clusters within the data. Additionally, it requires no special initialization, as it can start with the entire data in a single mixed class and split down to an appropriate level. The final class partition has k classes with associated K-Wishart parameters for each class.

7. CLASSIFICATION RESULTS

In this study, we obtained unsupervised clustering of the sample covariance matrix data using the K-Wishart classifier with different number of classes (it varies from 4 to 11 classes). Fig. 3 shows 2 examples of K-Wishart clustering (top) for 5 and 7 classes (left and right, respectively) with class histograms (below). The class histograms are 1-D compactions of covariance matrix samples that can be used to visualize the goodness-of-fit to the models [9].

7.1. Classification accuracy

As it was mentioned, we have classified images with different number of classes. We now merge these classification classes into four major ground truth classes (firn, superimposed ice, glacier ice and Herringbone ice), using the GPR ground truth profiles.

Fig. 4 is as an example where the number of classes in the original classified image has been reduced into 4 major classes and GPR data profiles have been overlaid on merged classified image.

We investigate the effect of acquisition conditions on the classification accuracy compared to the ground truth classes. Fig. 5 shows the results of K-Wishart classification accuracy (%) for different incidence angles by keeping other parameters fixed.

This preliminary investigation shows more consistent results for middle incidence angles (IS3-IS6) with different orbits and polarizations and it is expected to get better classifications and less variability. But there is no clear preference for HHHV or VVVH polarization and ascending or descending orbit.

Some results for the K-Wishart unsupervised classification reduced into 4 major classes with different parameter acquisitions are shown in Fig. 6. As can be seen, the main confusion seems to be at herringbone/glacier ice boundary. In most cases the firn/superimposed ice boundary is recognizable which is more important for glaciology studies.

7.2. Classification consistency

We characterize the consistency of the classification as the firn area total variation between two images to obtain the expected variation of firn area boundary with superimposed ice zone. Table 1 is list of omission errors of firn line for different pairs which is an indicator of variability of this boundary. We obtained the total variation of about 10.08% $\pm$ 2.69% and this variation is only due to classification. Note that this is for the worst case of mixed acquisition conditions. The differences between two classified images can only be considered significant when compared to that of the classification total variation.

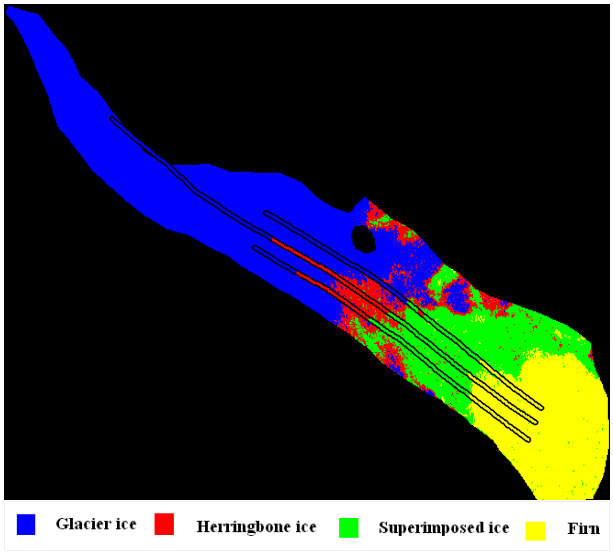

Figure 4. The merged classified image of the 4 major ground truth classes with GPR data line overlaid.

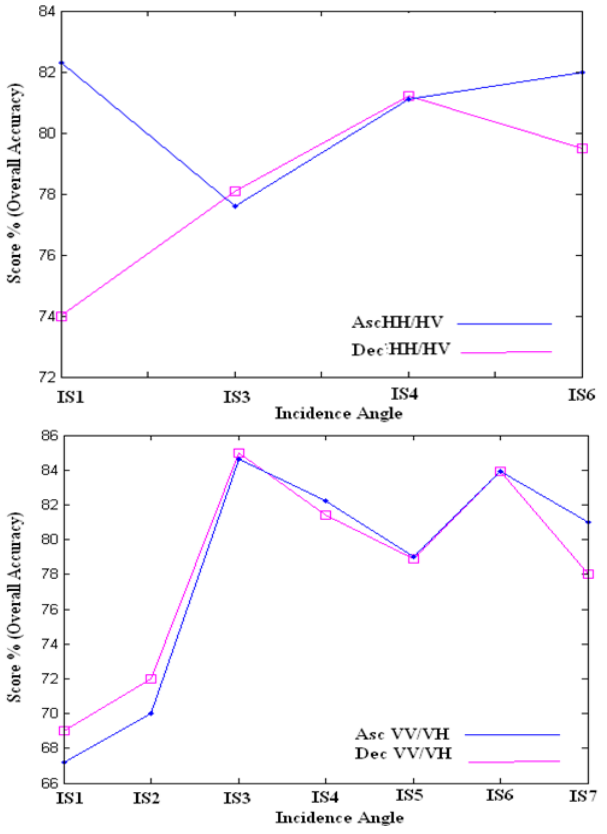

Figure 5. The results of K-Wishart classification accuracy (%) for different incidence angles, by fixing other parameters, showing more consistent results for middle incidence angles (IS3-IS6).

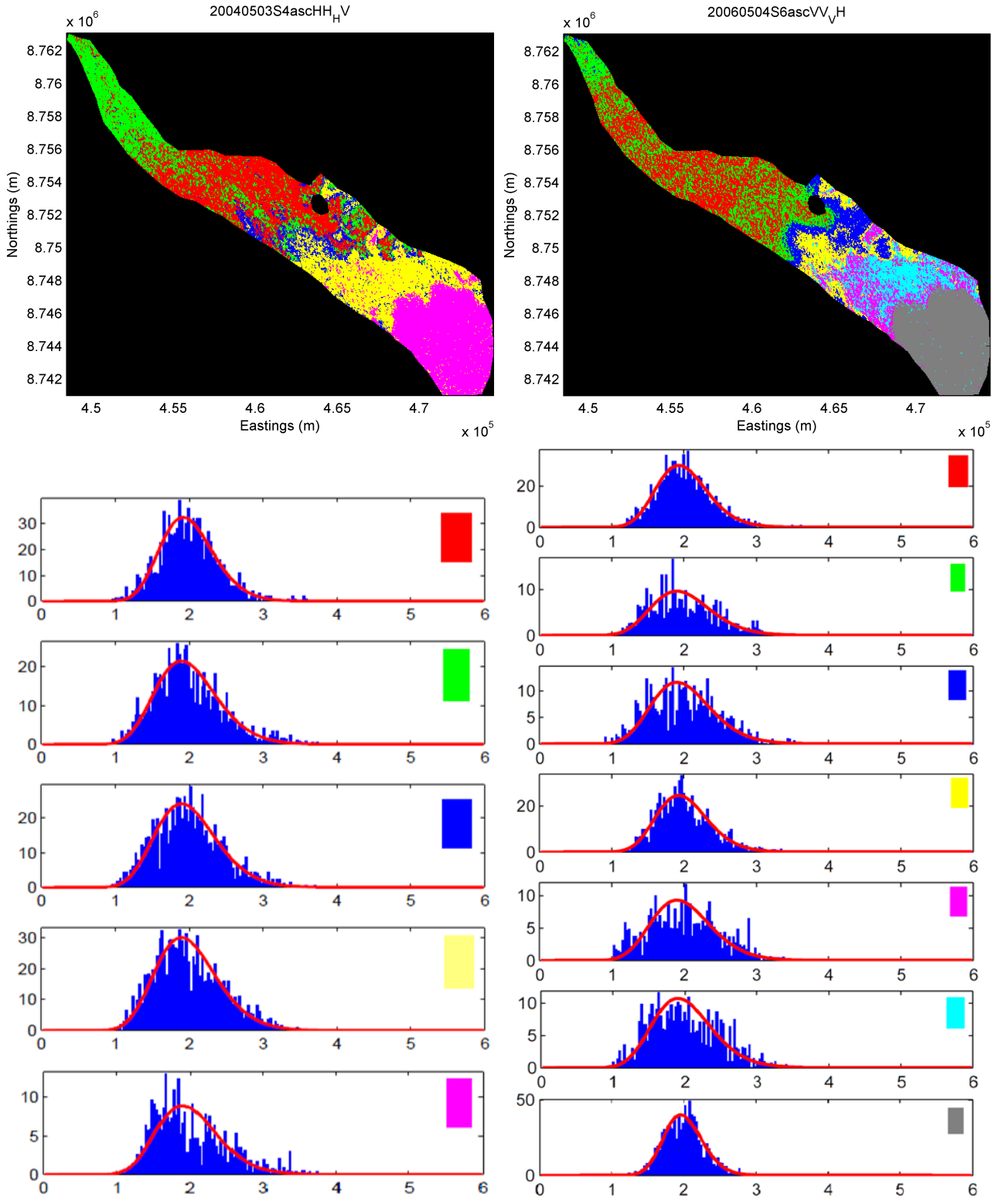

Figure 3. Unsupervised classification images (shown on a UTM grid projection) from K-Wishart clustering (top) for 5 classes (left) and 7 classes (right) with class histograms (below).

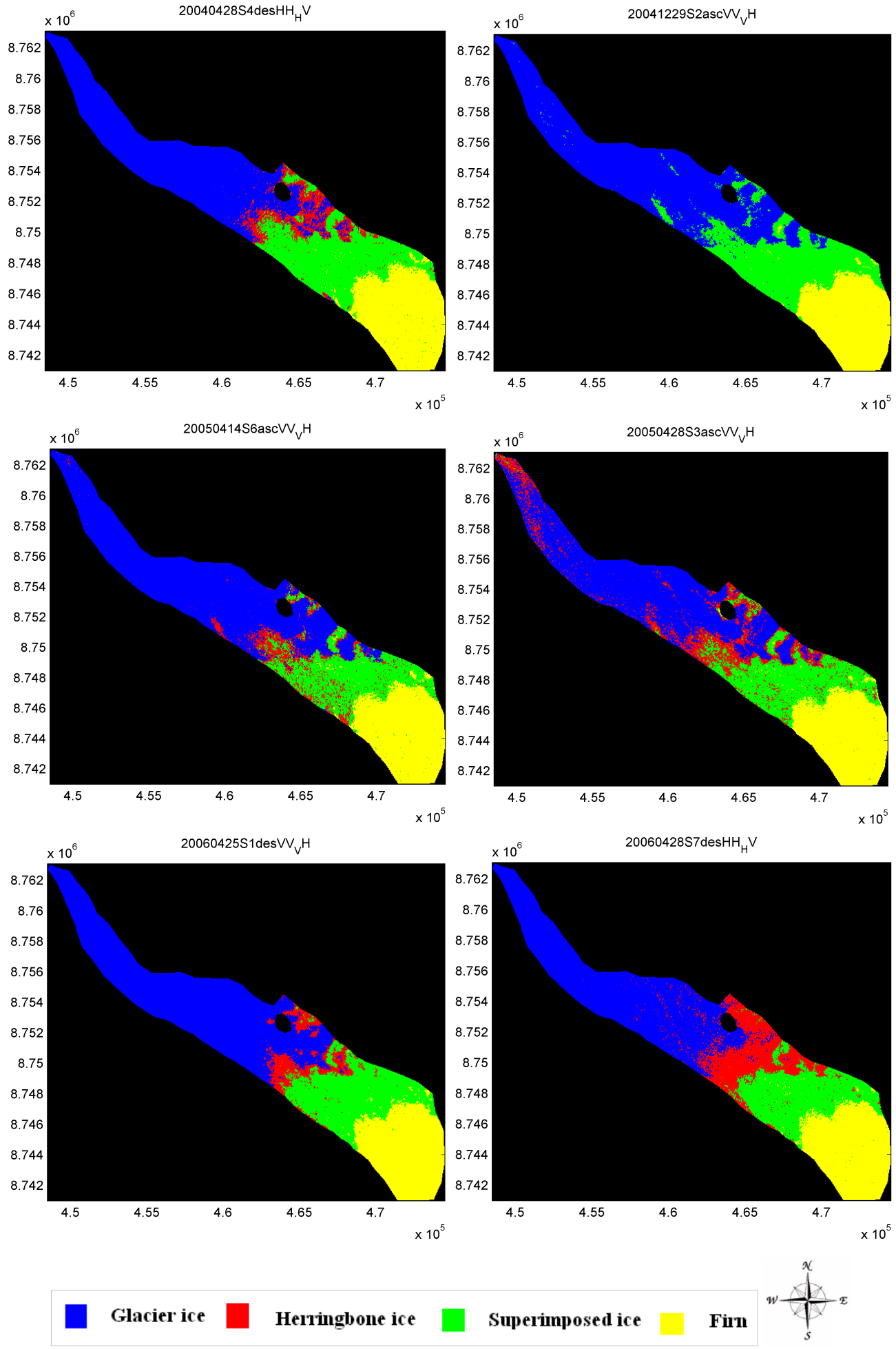

Figure 6. Some reduced classification results showing the variation with different acquisition conditions.

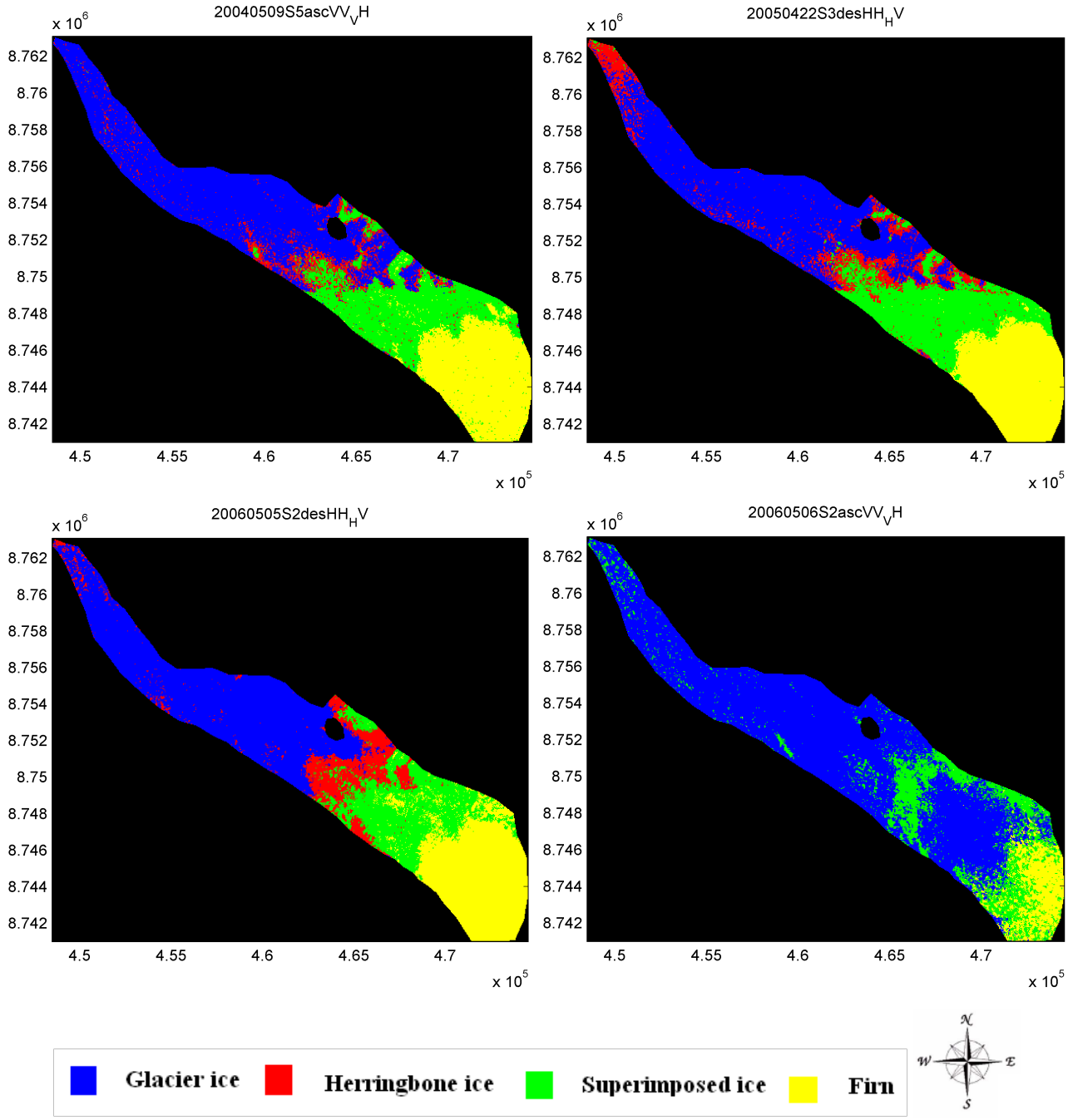

Figure 7. Images for change detection : 2004, 2005, 2006 and rain image from 2006

Table 1. The variation of Firn area for some pairs

Image 1	Image 2	Total Error
20040405S5decHH/HV	20040428S2ascVV/VH	10.45%
20040405S5decHH/HV	20050309S2ascVV/VH	13.65%
20040405S5decHH/HV	20050415S4ascVV/VH	11.79 %
20040405S5decHH/HV	20060412S7decVV/VH	14.39 %
20040428S2ascVV/VH	20050309S2ascVV/VH	8.90%
20040428S2ascVV/VH	20050415S4ascVV/VH	7.52%
20040428S2ascVV/VH	20060412S7decVV/VH	11.56%
20050309S2ascVV/VH	20050415S4ascVV/VH	6.95%
20050309S2ascVV/VH	20060412S7decVV/VH	7.4%
20050415S4ascVV/VH	20060412S7decVV/VH	8.22%

Table 2. Total error of Firn for change detection images

Image 1	Image 2	Total Error
20040509S5ascVV/VH	20050422S3decVV/VH	5.50%
20040509S5ascVV/VH	20060505S2decHH/HV	8.72%
20050422S3decVV/VH	20060505S2decHH/HV	7.31%
20060505S2decHH/HV	20060506S2ascVV/VH	65.2%

8. POST-CLASSIFICATION CHANGE DETECTION

After dealing with consistency by comparing scenes close together in time and from different acquisition parameters, we may now discuss subsequent yearly classifications in terms of post-classification change detection by directly observing differences in the classified images and obtaining the variation of firn area for each pair of images.

Fig. 7 shows images for change detection from 2004, 2005, 2006. Table 2 indicates measure of variations of firn area between two images. The total variation of firn area found between 2004 and 2006 do not exceed the expected classification variation, which indicates insignificant change for this period. However, one image (the last row in Table 2, $20060506S2ascVV/VH$) shows a significant change of 65.2% compared to the day before. Kongsvegen is known to be a slow moving glacier and so changes at this scale are not expected. The last image coincided with the onset of rain in the meteorological records, which explains the change because wet snow has a markedly different backscatter response to cold dry snow.

9. CONCLUSIONS

This study presented non-Gaussian clustering of Arctic glacier, Kongsvegen, using Envisat ASAR images with different acquisition parameters. The highest classification accuracy, compared to ground truth, was around 84% for IS3 VVVH Descending. We characterized the consistency of the classification as the firn area total variation between two images to obtain the expected variation just due to classification. The variation found between 2004 and 2006 did not exceed the expected classification variation and we cannot detect significant change for this period. However, an image taken after the onset of rain clearly showed significant change compared to the day before. Hence, images acquired during wet conditions must be avoided. We will study on the statistical interpretation of mixed acquision configurations with more samples in future.

ACKNOWLEDGEMENTS

The authors would like to thanks NORUT, Tromsø for the data set and geocoding software.

REFERENCES

[1] S. Solomon, D. Qin, M. Manning, Z. Chen, M. Marquis, K.B. Averyt, M. Tignor, and H.L. Miller. *IPCC, 2007: Climate Change 2007: The Physical Science Basis. Contribution of Working Group I to the Fourth Assessment Report of the Intergovernmental Panel on Climate Change*. Cambridge University Press, Cambridge, United Kingdom and New York, NY, USA., 2007.

[2] E. Jakeman and P. N. Pusey. A model for non-Rayleigh sea echo. *IEEE Trans. Antennas Propagat.*, 24, 6:806–814, November 1976.

[3] J. S. Lee, D. L. Schuler, R. H. Lang, and K. J. Ranson. K-distribution for multi-look processed polarimetric sar imagery. In *IEEE Int. Geosci. Remote Sensing Symp.*, pages 2179–2181, 1994.

[4] A. P. Doulgeris and T. Eltoft. Scale mixture of gaussian modelling of polarimetric sar data. *EURASIP Journal on Advances in Signal Processing*, 2010(874592):12, 2010.

[5] Corina C. Freitas, Alejandro C. Frery, and Antonio H. Correia. The polarimetric G distribution for SAR data analysis. *Environmetrics*, 16:13–31, 2005.

[6] K. Langley, S.-E. Hamran, K. A. Høgda, O. Brandt R. Storvold, J. Kohler, and J. O. Hagen. From glacier facies to sar backscatter zones via gpr. *IEEE Transactions on Geoscience and Remote Sensing*, Submitted, 2007.

[7] C. Oliver and S. Quegan. *Understanding Synthetic Aperture Radar Images*. SciTech Publishing, Raleigh, USA, 2nd edition, 2004.

[8] A. P. Doulgeris, S.N. Anfinsen, and T. Eltoft. Classification with a non-gaussian model for polsar data. *Geoscience and Remote Sensing, IEEE Transactions on*, 46(10):2999–3009, Oct. 2008.

[9] A. P. Doulgeris, S.N. Anfinsen, Y. Larsen, K. Langley, and T. Eltoft. Evaluation of polarimetric configurations for glacier classification. In *International POLinSAR Workshop*, Frascati, Italy, January 26-30 2009.

[10] A. P. Dempster, N. M. Laird, and D. B. Rubin. Maximum likelihood from incomplete data via teh EM algorithm. *Journal of the Royal Statistical Society. Series B*, 39(1):1–38, 1977.

[11] A. P. Doulgeris and T. Eltoft. Automated Non-Gaussian clustering of polarimetric SAR. In *8th European Conference on Synthetic Aperture Radar (EUSAR)*, Aachen, Germany, 2010.